PHYSICAL REVIEW LETTERS

Voltage-Induced Ferromagnetic Resonance in Magnetic Tunnel Junctions

Jian Zhu,[1] J. A. Katine,[2] Graham E. Rowlands,[1] Yu-Jin Chen,[1] Zheng Duan,[1] Juan G. Alzate,[3] Pramey Upadhyaya,[3] Juergen Langer,[4] Pedram Khalili Amiri,[3] Kang L. Wang,[3] and Ilya N. Krivorotov[1]

[1]*Department of Physics and Astronomy, University of California, Irvine, California 92697, USA*
[2]*Hitachi Global Storage Technologies, 3403 Yerba Buena Road, San Jose, California 95135, USA*
[3]*Department of Electrical Engineering, University of California, Los Angeles, California 90095, USA*
[4]*Singulus Technologies, 63796 Kahl am Main, Germany*
(Received 31 August 2011; revised manuscript received 31 January 2012; published 9 May 2012)

We demonstrate excitation of ferromagnetic resonance in CoFeB/MgO/CoFeB magnetic tunnel junctions (MTJs) by the combined action of voltage-controlled magnetic anisotropy (VCMA) and spin transfer torque (ST). Our measurements reveal that GHz-frequency VCMA torque and ST in low-resistance MTJs have similar magnitudes, and thus that both torques are equally important for understanding high-frequency voltage-driven magnetization dynamics in MTJs. As an example, we show that VCMA can increase the sensitivity of an MTJ-based microwave signal detector to the sensitivity level of semiconductor Schottky diodes.

Excitation of subnanosecond magnetic dynamics by an electric field is a grand challenge in the field of spintronics. The ability to perform high-speed manipulation of magnetization by electric fields rather than by current-induced spin torques or magnetic fields would greatly reduce Ohmic losses and thereby improve the performance of spintronic devices such as nonvolatile magnetic memory. In this Letter we demonstrate the excitation of GHz-range magnetization dynamics in nanoscale MTJs by the combined action of ST arising from spin-polarized current [1–9] and VCMA induced by electric field [10–20]. We show that ST and VCMA torques have similar magnitudes in MTJs with ultrathin ($<$ 1 nm) tunnel barriers for both DC and microwave-frequency voltages. Our results demonstrate that a description of voltage-induced high-speed magnetic dynamics in MTJs should generally include not only ST but also VCMA terms. As an example, we show that VCMA can increase the sensitivity of a ST microwave signal detector, raising it to the sensitivity level of semiconductor Schottky diodes.

We make measurements of voltage-driven magnetization dynamics in 150×70 nm^2 elliptical MTJ nanopillars shown schematically in Fig. 1. The nanopillars are patterned by ion milling from (bottom lead)/ Ta(5)/ PtMn(15)/Co$_{70}$Fe$_{30}$(2.3)/Ru(0.85)/Co$_{40}$Fe$_{40}$B$_{20}$(2.4)/ MgO(0.83)/Co$_{20}$Fe$_{60}$B$_{20}$(1.58)/Ta(5)/(cap) multilayer (thicknesses in nm) with resistance-area product of 3.5 $\Omega \cdot \mu$m^2 deposited by magnetron sputtering in a Singulus TIMARIS system. Prior to patterning, the multilayers are annealed for 2 h at 300°C in a 1 T in-plane magnetic field that sets the pinned layer exchange bias direction parallel to the long axis of the nanopillars (the $\hat{x}$ axis of our Cartesian coordinate system). The Co$_{20}$Fe$_{60}$B$_{20}$ free layer exhibits perpendicular magnetic anisotropy [21], and the

equilibrium direction of its magnetization at zero field is normal to the sample plane ($\hat{z}$ axis). Measurements of the nanopillar conductance G versus $\hat{x}$-axis magnetic field H_x (defined as the sum of the external $\hat{x}$-axis field and the stray field from the polarizer) confirm the out-of-plane orientation of the free layer magnetization at $H_x = 0$ (see Fig. 1). The MTJ conductance exhibits cosine dependence on the angle ϕ between the magnetic moments of the free and pinned layers [22]:

$$G = G_0(1 + P^2 \cos(\phi)), \qquad (1)$$

where P is the current spin polarization. It follows that the shape of the $G(H_x)$ curve is identical to that of the $M_x(H_x) = M_s \cos(\phi)$ hysteresis loop, where M_s is saturation magnetization of the free layer and M_x is projection of magnetization onto the $\hat{x}$ axis. The $G(H_x)$ curves in Fig. 1 are hard-axis hysteresis loops, the slopes of which depend on the applied direct voltage bias V_{dc} by virtue of VCMA [17–20]. As discussed in the supplementary online material [23], ST from V_{dc} does not significantly affect the $G(H_x)$ hysteresis loop.

The effective perpendicular magnetic anisotropy energy per unit volume of the free layer, E_p, includes magneto-crystalline, surface, and magnetostatic anisotropy contributions and can be calculated from the area under the hysteresis loop $M_x(H_x)$ in Fig. 1:

$$E_p = \int_0^{M_s} H_x(M_x)dM_x = \frac{1}{2}M_sH_p, \qquad (2)$$

where H_p is the effective perpendicular anisotropy field. The inset in Fig. 1 displays the variation of the perpendicular anisotropy field with dc voltage $\Delta H_p(V_{dc}) = H_p(V_{dc}) - H_p(0)$. This dependence is well fit by a straight line with the slope of 0.6 kOe/V, which corresponds to magnetic anisotropy energy per area per electric field
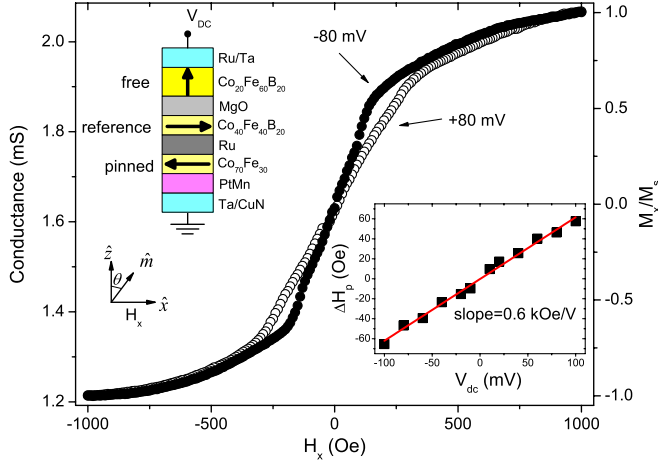
FIG. 1 (color online). Hysteresis loop of MTJ conductance G versus in-plane magnetic field H_x measured under ± 80 mV direct voltage bias V_{dc}. The left inset shows schematic of the MTJ nanopillar. The right inset displays variation of the effective perpendicular anisotropy field $\Delta H_p(V_{dc})$ with DC voltage extracted from the $G(H_x)$ hysteresis loops via Eq. (2) (squares) and a linear fit to the data (line).

FIG. 2 (color online). Rectified voltage V_{mix} versus frequency f of the applied microwave signal measured at several values of the in-plane magnetic field H_x. The FMR response curves $V_{mix}(f)$ at different fields are vertically offset by 0.06 mV. At $H_x = 0$, $V_{mix}(f)$ is a symmetric Lorentzian curve, while at $|H_x| > 0$, $V_{mix}(f)$ is a sum of symmetric and antisymmetric Lorentzians. The antisymmetric part of $V_{mix}(f)$ changes sign upon reversal of H_x, while the symmetric part is negative for any H_x.

of 37 fJ/(V · m). This value is similar to the magnitude of VCMA reported by other groups [15,17].

We study the effect of high-frequency voltage oscillations on magnetization of the MTJ free layer using a ferromagnetic resonance (FMR) technique. In this technique, magnetization oscillations are excited by a microwave voltage applied to the MTJ, and the amplitude of magnetization precession is detected electrically via the rectified voltage V_{mix} generated by the MTJ [24,25]. This technique is commonly called spin torque FMR (ST-FMR), since the magnetization precession of the free layer is driven by ST from the microwave current $I_{ac}\cos(2\pi ft)$ flowing through the MTJ [26]. However, as we show below, magnetization oscillations in our MTJ samples are excited not only by ST from I_{ac} but also by oscillating VCMA induced by the applied microwave voltage V_{ac}. In this method, the rectified voltage $V_{mix} = \frac{1}{2}I_{ac}R_{ac}\cos(\psi)$ arises from mixing of the microwave current $I_{ac}\cos(2\pi ft)$ and tunneling magnetoresistance oscillations $R_{ac}\cos(2\pi ft + \psi)$ resulting from the free layer's magnetization precession [25]. We sweep the microwave drive frequency f and measure ST-FMR response curve $V_{mix}(f)$. In general, peaks in the $V_{mix}(f)$ response curve arise from resonant excitation of spin wave eigenmodes of the MTJ, and analysis of the line shape of these ST-FMR resonances gives the value of Gilbert damping and the magnitude of voltage-induced torques (including ST) acting on magnetization [26].

The measured dependence of $V_{mix}(f)$ is shown in Fig. 2 for several values of H_x. The negative peaks in $V_{mix}(f)$ arise from excitation of the quasiuniform FMR mode of the free layer [25]. For all measurements, the applied microwave power is -36 dBm, which is small enough to
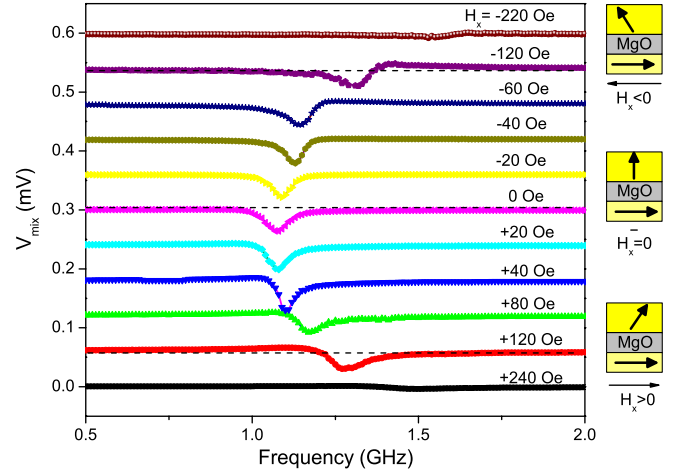
excite the free layer precession in the linear regime. At $H_x = 0$, the magnetization of the free layer is perpendicular to the sample plane ($\theta = 0$), and the ST-FMR line shape $V_{mix}(f)$ is well described by a symmetric Lorentzian. For nonzero H_x, the magnetization of the free layer is tilted away from the sample normal, and $V_{mix}(f)$ develops asymmetry. In this regime, the ST-FMR line shape is well fit by a sum of symmetric and antisymmetric Lorentzians with identical resonance frequencies f_0:

$$V_{mix}(f) = \frac{V_s}{1 + (f - f_0)^2/\sigma^2} + \frac{V_a(f - f_0)/\sigma}{1 + (f - f_0)^2/\sigma^2}, \quad (3)$$

where V_s and V_a are the symmetric and antisymmetric term amplitudes, and σ is the half width at half maximum. As is evident from Fig. 2 (compare ST-FMR curves at $H_x = \pm 120$ Oe), the antisymmetric part of the ST-FMR line shape, V_a, changes sign upon reversal of H_x.

The symmetric component of the ST-FMR curve arises from in-plane ST $\vec{\tau}_i \sim \hat{\mathbf{m}} \times (\hat{\mathbf{e}}_p \times \hat{\mathbf{m}})$ that lies in the plane defined by the magnetic moments of the free and the pinned layers, where $\hat{\mathbf{m}}$ is the unit vector in the direction of the free layer's magnetization and $\hat{\mathbf{e}}_p$ is the unit vector in the direction of the polarizer's magnetization. An antisymmetric component of the ST-FMR curve has been previously observed in nanoscale MTJs at nonzero DC bias voltages, and was shown to arise from a fieldlike ST, $\vec{\tau}_f \sim \hat{\mathbf{m}} \times \hat{\mathbf{e}}_p$ [27,28]. The antisymmetric component was observed to vanish at zero bias voltage, which was explained by quadratic dependence of $\vec{\tau}_f$ on the voltage bias [27].

Hence, our observation of a nonzero antisymmetric component of the ST-FMR response curve at zero dc voltage is surprising.

In order to understand the origin of the ST-FMR line shape asymmetry in our MTJ system, we numerically simulate [23] the resonance curve by solving the Landau-Lifshitz-Gilbert equation of motion of the free layer in the macrospin approximation [29]:

$$\frac{d\hat{\mathbf{m}}}{dt} = -\gamma\hat{\mathbf{m}} \times \vec{H}_{\mathrm{eff}} + \alpha\hat{\mathbf{m}} \times \frac{d\hat{\mathbf{m}}}{dt}$$
$$-\gamma\frac{J\hbar}{2eM_s d}\frac{P}{1 + P^2\cos(\phi)}$$
$$\times [\hat{\mathbf{m}} \times (\hat{\mathbf{m}} \times \hat{\mathbf{e}}_p) + b_f\hat{\mathbf{m}} \times \hat{\mathbf{e}}_p]. \quad (4)$$

In Eq. (4), $\vec{H}_{\mathrm{eff}}$ is the effective field including contributions from the external, magnetostatic, and perpendicular magnetic anisotropy fields, γ is the gyromagnetic ratio, α is the Gilbert damping parameter, $J\hbar/2e$ is the microwave spin current density, d is the thickness of the free layer, and b_f is the ratio of the magnitudes of the in-plane ST and fieldlike ST.

For the approximately quadratic dependence of $\vec{\tau}_f$ on the current bias observed in previous experiments [27,28,30], b_f is proportional to J and thus $\vec{\tau}_f$ can be neglected at zero current bias. However, we include $\vec{\tau}_f$ in the simulations since a linear dependence of $\vec{\tau}_f$ on current (corresponding to $b_f = \mathrm{const}$) is, in principle, possible for MTJs with different free and pinned ferromagnetic layers [31]. Such a linear dependence of $\vec{\tau}_f$ on current would give rise to an antisymmetric component of the ST-FMR response curve at zero bias.

In our simulations, both the charge current density $J = J_0\sin(2\pi f t)$ and the effective magnetic field $\vec{H}_{\mathrm{eff}}$ are generally time dependent. The time-dependence of the effective magnetic field arises from the VCMA, giving the time-dependent perpendicular anisotropy field $H_{\perp z} = (H_{\perp 0} + \Delta H_\perp\sin(2\pi f t))\cos(\theta)$, where $H_{\perp 0}$ is the anisotropy field at zero bias and $\Delta H_\perp$ is the VCMA field. The simulated ST-FMR response curves shown in Fig. 3(a) are calculated assuming nonzero in-plane ST and nonzero VCMA ($\Delta H_\perp = 4$ Oe), but zero fieldlike ST($b_f = 0$). In these simulations, we use $H_{\perp 0} = 11\,362$ Oe, $\alpha = 0.030$, and $P = 0.54$ as determined by fitting the resonance frequency, the line width and the amplitude of the ST-FMR resonance curve measured at $H_x = 0$. Allowing for uncertainty in the sample volume, we note that $P = 0.54$ agrees well with the value $P = 0.52$ calculated from the MTJ conductance using Eq. (1). In the simulations, we use demagnetization factors $N_x = 0.014$, $N_y = 0.040$, $N_z = 0.946$ obtained from the assumption that the free layer is an elliptic cylinder [32]. The saturation magnetization M_s is taken to be 950 emu/cm³ as measured by vibrating sample magnetometry, and $\Delta H_\perp = 4$ Oe is calculated from the slope of $\Delta H_p(V_{\mathrm{dc}})$ line in the inset of
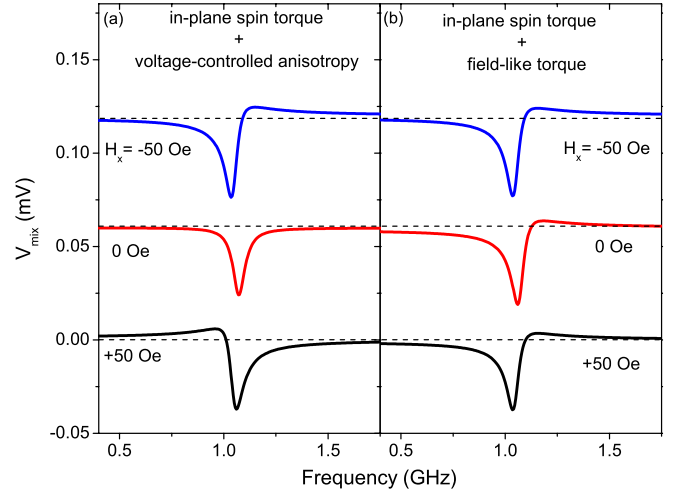

FIG. 3 (color online). Macrospin simulations of ST-FMR line shape assuming nonzero in-plane ST and (a) nonzero VCMA ($\Delta H_\perp = 4$ Oe) and zero fieldlike ST ($b_f = 0$), (b) zero VCMA ($\Delta H_\perp = 0$ Oe) and nonzero fieldlike ST ($b_f = 0.5$). The curves for different values of H_x are vertically offset by 0.06 mV.

Fig. 1. Figure 3(a) shows that the simulated ST-FMR line shapes reproduce the symmetry of the measured curves: (i) the line shape is symmetric at $H_x = 0$ and (ii) the line shape is asymmetric with the antisymmetric part changing sign upon reversal of H_x for $|H_x| > 0$. In contrast, simulations with a nonzero fieldlike torque $\vec{\tau}_f$ do not reproduce the symmetry of the measured line shapes. Figure 3(b) shows the simulation results for nonzero in-plane ST and nonzero fieldlike ST ($b_f = 0.5$) but zero VCMA ($\Delta H_\perp = 0$). The simulated ST-FMR line shapes are asymmetric for all applied field values, and the sign of the antisymmetric part does not depend on the applied field direction. Therefore, our simulations demonstrate that the observed ST-FMR line shape asymmetry arises from VCMA, not fieldlike ST.

The antisymmetric part of the ST-FMR line shape calculated with the VCMA value derived from dc measurements ($\Delta H_\perp = 4$ Oe) has similar magnitude to that of the measured ST-FMR response curve. This implies that the magnitude of VCMA is comparable for microwave and DC voltages. Since the measured magnitudes of the symmetric and antisymmetric parts of the ST-FMR line shapes are similar for $\theta \neq 0$, we conclude that ST and VCMA torque generally have similar magnitudes in our MTJs.

Although the ST-FMR line shape is well reproduced by the simulations with the VCMA drive term, the dependence of the simulated resonance frequency f_0 on H_x does not qualitatively agree with the measurements. The macrospin simulations predict decreasing f_0 with increasing $|H_x|$ as shown in Figs. 4(a) and 4(c), while the measured $f_0(|H_x|)$ shows the opposite trend (Fig. 2). We find that this discrepancy arises from the simplified form of the perpendicular anisotropy energy used in the simulations.
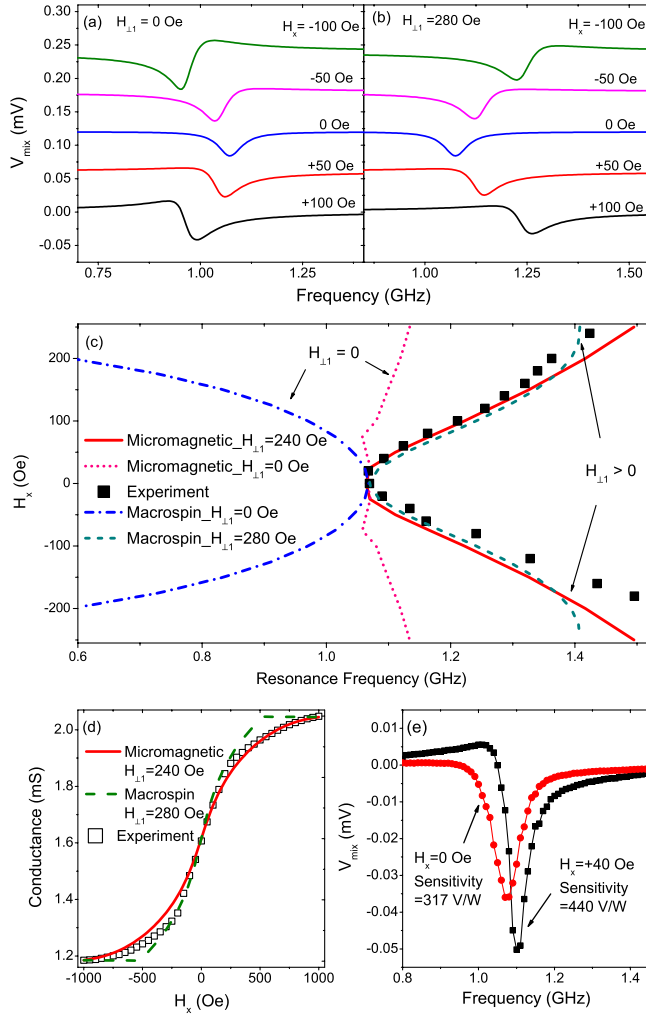
FIG. 4 (color online). Macrospin simulations of ST-FMR response curves with (a) zero ($H_{\perp 1} = 0$) and (b) positive ($H_{\perp 1} = 280$ Oe) second-order perpendicular anisotropy. The curves are vertically offset by 0.06 mV. (c) Macrospin and micromagnetic simulations of ST-FMR resonance frequency versus H_x for zero and positive $H_{\perp 1}$ (lines) shown together with the experimental data (solid squares). (d) Macrospin and micromagnetic simulations (lines) of the $G(H_x)$ hysteresis loop using the magnetic anisotropy parameters given by the best fits in (c). Squares are experimental data measured at zero bias voltage. (e) Sensitivity of the MTJ to a microwave signal is enhanced by VCMA when the free layer magnetization is tilted from the sample normal by magnetic field $H_x = +40$ Oe.

The thickness of the free layer in our samples is intentionally tuned to a value at which the uniaxial perpendicular anisotropy and the easy-plane shape anisotropy have comparable magnitudes but opposite signs. Therefore, the leading terms proportional to $\sin^2(\theta)$ in the angular dependence of both anisotropy energy expansions nearly cancel each other and the higher order term proportional to $\sin^4(\theta)$ becomes important [33].

In order to study the impact of the second-order perpendicular anisotropy term on $f_0(H_x)$, we repeat our macrospin simulations with nonzero first- and second-order perpendicular anisotropy terms: $E_\perp = K_1 \sin^2(\theta) + K_2 \sin^4(\theta)$, which gives $H_{\perp z} = [H_{\perp 0} + H_{\perp 1}(1 - \cos^2(\theta))]\cos(\theta)$ at zero bias, where $H_{\perp 0} = 2K_1/M_s$ and $H_{\perp 1} = 4K_2/M_s$. Our simulations show that adding a small positive second-order anisotropy field $H_{\perp 1}$ changes the shift of the resonance frequency with $|H_x|$ from negative to positive, and the results from simulations at $H_{\perp 1} = 280$ Oe are in good quantitative agreement with the measured $f_0(H_x)$ [Figs. 4(b) and 4(c)].

We also make micromagnetic simulations of $f_0(H_x)$ using MICROMAGUS simulator and find the micromagnetic $f_0(H_x)$ to be in qualitative agreement with the macrospin simulation results. Figure 4(c) shows that micromagnetic simulations performed with $H_{\perp 1} = 0$ give $f_0(H_x)$ inconsistent with the experimental data, while those performed with $H_{\perp 0} = 11\,515$ Oe and $H_{\perp 1} = 240$ Oe reproduce the measured $f_0(H_x)$ well. Micromagnetic and macrospin simulations of the $G(H_x)$ hysteresis loop made with the values of $H_{\perp 0}$ and $H_{\perp 1}$ obtained from best fits of $f_0(H_x)$ are also in good agreement with the experimental data as shown in Fig. 4(d).

The measured amplitudes of the symmetric and antisymmetric parts of the ST-FMR line shape are similar to each other for $|H_x| > 0$. This implies that the magnitude of VCMA torque is similar to that of ST, and thus both torques are important for the description of voltage-driven magnetization dynamics in MTJs, such as ST-induced magnetization reversal [34,35]. As an example, Fig. 4(e) shows that VCMA can significantly increase the sensitivity of an MTJ-based microwave signal detector [24]. Indeed, the maximum rectified voltage generated by the MTJ in response to applied microwave signal increases by 39% when H_x increases from 0 Oe to +40 Oe [23]. This increase in the detector sensitivity is mainly due to the antisymmetric part of the ST-FMR line shape, which is induced by VCMA. With the VCMA contribution, the MTJ microwave detector sensitivity reaches 440 V/W—a value similar to that of semiconductor Schottky diodes ($\sim 5 \times 10^2$ V/W [36]).

In conclusion, we demonstrate excitation of GHz-range magnetization dynamics in nanoscale MTJs by the combined action of spin torque and voltage-controlled magnetic anisotropy. Our work shows that the magnitudes of high-frequency spin torque and voltage-controlled magnetic anisotropy torque in MgO-based MTJs can be similar to each other, and thus that quantitative descriptions of voltage-driven magnetization dynamics in MTJs should generally include both torque terms. We show that voltage-controlled magnetic anisotropy can increase the sensitivity of spin torque MTJ microwave signal detectors to the sensitivity level of Schottky diode detectors.

[1] J. C. Slonczewski, J. Magn. Magn. Mater. **159,** L1 (1996).
[2] L. Berger, Phys. Rev. B **54,** 9353 (1996).
[3] J. A. Katine, F. J. Albert, R. A. Buhrman , E. B. Myers and D. C. Ralph, Phys. Rev. Lett. **84,** 3149 (2000).
[4] M. Tsoi, A. G. M. Jansen, J. Bass, W.-C. Chiang, V. Tsoi, and P. Wyder, Nature (London) **406,** 46 (2000).
[5] J. Grollier, V. Cros, A. Hamzic, J. M. George, H. Jaffrès, A. Fert, G. Faini, J. Ben Youssef, and H. Legall, Appl. Phys. Lett. **78,** 3663 (2001).
[6] S. I. Kiselev, J. C. Sankey, I. N. Krivorotov, N. C. Emley, R. J. Schoelkopf, R. A. Buhrman, and D. C. Ralph, Nature (London) **425,** 380 (2003).
[7] S. Urazhdin, N. O. Birge, W. P. Pratt, Jr., and J. Bass, Phys. Rev. Lett. **91,** 146803 (2003).
[8] W. H. Rippard, M. R. Pufall, S. Kaka, S. E. Russek, and T. J. Silva, Phys. Rev. Lett. **92,** 027201 (2004).
[9] I. N. Krivorotov, N. C. Emley, J. C. Sankey, S. I. Kiselev, D. C. Ralph and R. A. Buhrman, Science **307,** 228 (2005).
[10] T. Maruyama *et al.*, Nature Nanotech. **4,** 158 (2009).
[11] K. Nakamura, R. Shimabukuro, Y. Fujiwara, T. Akiyama, and T. Ito, and A. J. Freeman, Phys. Rev. Lett. **102,** 187201 (2009).
[12] D. Chiba, Y. Nakatani, F. Matsukura, and H. Ohno, Appl. Phys. Lett. **96,** 192506 (2010).
[13] M. K. Niranjan, C.-G. Duan, S. S. Jaswal, and E. Y. Tsymbal, Appl. Phys. Lett. **96,** 222504 (2010).
[14] Y. Shiota, T. Maruyama, T. Nozaki, T. Shinjo, M. Shiraishi, and Y. Suzuki, Appl. Phys. Express **2,** 063001 (2009).
[15] M. Endo, S. Kanai, S. Ikeda, F. Matsukura, and H. Ohno, Appl. Phys. Lett. **96,** 212503 (2010).
[16] S. Ha, N.-H. Kim, S. Lee, C.-Y. You, Y. Shiota, T. Maruyama, T. Nozaki, and Y. Suzuki, Appl. Phys. Lett. **96,** 142512 (2010).
[17] T. Nozaki, Y. Shiota, M. Shiraishi, T. Shinjoand Y. Suzuki, Appl. Phys. Lett. **96,** 022506 (2010).
[18] Y. Shiota, S. Murakami, F. Bonell, T. Nozaki, T. Shinjo, and Y. Suzuki, Appl. Phys. Express **4,** 043005 (2011).
[19] W. Wang, M. Li, S. Hageman, and C. L. Chien, Nature Mater. **11,** 64 (2012).
[20] Y. Shiota T. Nozaki, F. Bonell, S. Murakami, T. Shinjo, and Y. Suzuki, Nature Mater. **11,** 39 (2012).
[21] S. Ikeda, K. Miura, H. Yamamoto, K. Mizunuma, H. D. Gan, M. Endo, S. Kanai, J. Hayakawa, F. Matsukura, and H. Ohno, Nature Mater. **9,** 721 (2010).
[22] J. C. Slonczewski, Phys. Rev. B **39,** 6995 (1989).
[23] See Supplemental Material at http://link.aps.org/supplemental/10.1103/PhysRevLett.108.197203 for more information.
[24] A. A. Tulapurkar, Y. Suzuki, A. Fukushima, H. Kubota, H. Maehara, K. Tsunekawa, D. D. Djayaprawira, N. Watanabe, and S. Yuasa, Nature (London) **438,** 339 (2005).
[25] J. C. Sankey, P. M. Braganca, A. G. F. Garcia, I. N. Krivorotov, R. A. Buhrman, and D. C. Ralph, Phys. Rev. Lett. **96,** 227601 (2006).
[26] D. C. Ralph, Y.-T. Cui, L. Q. Liu, T. Moriyama, C. Wang, and R. A. Buhrman, Phil. Trans. R. Soc. A **369,** 3617 (2011).
[27] J. C. Sankey, Y.-T. Cui, J. Z. Sun, J. C. Slonczewski, R. A. Buhrman, and D. C. Ralph, Nature Phys. **4,** 67 (2008).
[28] C. Wang, Y.-T. Cui, J. Z. Sun, J. A. Katine, R. A. Buhrman, and D. C. Ralph, Phys. Rev. B **79,** 224416 (2009).
[29] J. Sun and D. Ralph, J. Magn. Magn. Mater. **320,** 1227 (2008).
[30] C. Wang, Y.-T. Cui, J. A. Katine, R. A. Buhrman, and D. C. Ralph, Nature Phys. **7,** 496 (2011).
[31] S. Oh *et al.*, Nature Phys. **5,** 898 (2009).
[32] M. Beleggia, M. De Graef, Y. T. Millev, D. A. Goode, and G. Rowlands, J. Phys. D **38,** 3333 (2005).
[33] R. L. Stamps, L. Louail, M. Hehn, M. Gester, and K. Ounadjela, J. Appl. Phys. **81,** 4751 (1997).
[34] Y. Huai, F. Albert, P. Nguyen, M. Pakala, and T. Valet, Appl. Phys. Lett. **84,** 3118 (2004).
[35] G. D. Fuchs, N. C. Emley, I. N. Krivorotov, P. M. Braganca, E. M. Ryan, S. I. Kiselev, J. C. Sankey, D. C. Ralph, R. A. Buhrman, and J. A. Katine, Appl. Phys. Lett. **85,** 1205 (2004).
[36] S. Ishibashi *et al.*, Appl. Phys. Express **3,** 073001 (2010).